Adsorption of Atomic Hydrogen on Single-Walled Carbon Nanotubes

Kyung Ah Park,[†] Kwanyong Seo,[‡] and Young Hee Lee*[,†]

Department of Physics, Center for Nanotubes and Nanostructured Composites, Sungkyunkwan Advanced Institute of Nanotechnology, Sungkyunkwan University, Suwon 440-746, and the Department of Chemistry, KAIST, Daejeon 305-701, Korea

Received: January 6, 2005; In Final Form: March 9, 2005

We have investigated atomic and electronic structures of hydrogen-chemisorbed single-walled carbon nanotubes (SWCNTs) by density functional calculations. We have searched for relative stability of various hydrogen adsorption geometries with coverage. The hydrogenated SWCNTs are stable with coverage of H/C, $\theta \geq 0.3$. The circular cross sections of nanotubes are transformed to polygonal shapes with different symmetries upon hydrogen adsorption. We find that the band gap in carbon nanotubes can be engineered by varying hydrogen coverage, independent of the metallicity of carbon nanotubes. This is explained by the degree of sp^3 hybridization.

Introduction

Carbon nanotube (CNT) has unique one-dimensional characteristics in atomic and electronic structures from its small diameter of a few *nanometers* and chirality.[1−4] Extensive theoretical and experimental research has been done in various applications of CNTs.[5−8] Large surface area with diverse distributions of micropores and mesopores in the network and ample empty space inside CNTs have opened new application areas in energy storage such as secondary batteries, supercapacitors, and hydrogen storage.[9−12] Another potential application area is the electronics devices such as field emission displays, gas sensors, and nanotransistors.[13−16] Despite such diverse applicability, several limitations still exist for real applications. One difficulty is that it is practically impossible to control the chirality during the growth process at the present stage. Various posttreatments such as doping of alkali metals and adsorption of gas adsorbates have been attempted to modulate the electronic properties.[5,17−19]

Chemical functionalization of CNTs can change the atomic and electronic properties of nanotubes and may enhance the performance in hydrogen storage, secondary batteries, and supercapacitors.[20−23] Sidewall functionalization of the single-walled carbon nanotubes (SWCNTs) by atomic hydrogen leads to transforming electronic structures from metallic to semiconducting by removing π states near the Fermi level.[24] Formation of a rectifier by hydrogenating half of the metallic CNTs clearly shows both rectifying and gating effects at room temperature. This is clear evidence of band gap opening of metallic tubes by hydrogenation. Yet, no systematic prediction has been made for band gap engineering in carbon nanotubes in terms of hydrogen coverage.

Several theoretical researches for hydrogen-chemisorbed SWCNTs have been reported.[25−31] Bauschlicher has done cluster calculations to study hydrogen coverage dependence using the ONIOM (our own *N*-layered integrated molecular orbital and molecular mechanics) approach.[32] Half-coverage was more favorable than full coverage by 0.81 eV per hydrogen atom. Gülseren et al. reported various types of adsorption patterns at coverage of 0.5 on SWCNTs.[33] They also observed the band gap opening at dimer and chain types. A systematic study is required for the atomic and electronic structure changes on hydrogen coverage and particularly for the possibility of band gap engineering with CNTs.

In this paper, we focus on a systematic study of atomic and electronic structures of hydrogenated SWCNTs in terms of hydrogen coverage using a self-consistent charge-density functional tight-binding (SCC-DFTB) approach and density functional theory (DFT) within local density approximation (LDA). We find several stable geometries of hydrogenated nanotubes for coverage up to $\theta = 1.0$. At low coverage of $\theta < 0.5$, the circular cross section of CNTs becomes different polygonal shapes depending on coverage. The adsorption energy does not change appreciably at higher coverage of $\theta > 0.5$. We also find that the band gap engineering can be achieved by changing the hydrogen coverage. The largest band gap is obtained at half coverage, which is attributed to the formation of maximum sp^3 hybridization. Various adsorption patterns on coverage and their relative stabilities will be graphically demonstrated.

Theoretical Approaches

We use the SCC-DFTB method to optimize various geometries of hydrogenated SWCNTs. The SCC-DFTB method uses a basis of numerically obtained s, p, and d (s and p) atomic orbitals for carbon (hydrogen) atoms. Hamiltonian and overlap matrix elements are evaluated by a two-center approach. Charge transfer is taken into account through the incorporation of a self-consistent scheme for Mulliken charge based on the second-order expansion of the Kohn−Sham energy in terms of charge density fluctuations. The diagonal elements of the Hamiltonian matrix employed are then modified by the charge-dependent contributions to describe the change in the atomic potentials due to the charge transfer. The off-diagonal elements have additional charge-dependent terms due to the Coulomb potential of ions. They decay as $1/r$ and thus account for the Madelung energy of the system. This procedure optimizes not only the

* To whom correspondence should be addressed. E-mail: leeyoung@skku.edu.
† Sungkyunkwan University.
‡ Korea Advanced Institute of Science and Technology.

10.1021/jp0500743 CCC: $30.25 © 2005 American Chemical Society
Published on Web 04/05/2005

total energy but also an excess charge transfer that is usually overestimated in a conventional tight-binding approach. Further details of the SCC-DFTB method have been published elsewhere.[34]

We searched various hydrogen adsorption sites on nanotubes at different coverage with computationally less demanding SCC-DFTB calculations. Once we determine the optimized geometries by the SCC-DFTB method, we performed more accurate calculations using the LDA approach whenever necessary. We adopted the Vanderbilt ultrasoft pseudopotential for ionic potentials.[35] The exchange-correlation energy in LDA is parametrized by Perdew and Wang's scheme.[36] Electron Kohn−Sham wave functions are expanded in a planewave basis with a kinetic energy cutoff of 24 Ry.[37]

We choose (5,5) armchair and (9,0) zigzag nanotubes for our calculations. For SCC-DFTB calculations, we choose a supercell of eight layers with periodic boundary conditions along the tube axis. The diameter of the (5,5) nanotube after full relaxation with the SCC-DFTB is 6.8 Å, with an average bond length of 1.42 Å. The forces on each atom to be converged during each relaxation are less than 10^{-3} au. For LDA calculations, nanotubes are separated by 5.0 Å to neglect interactions between tubes in the bundle, and for hydrogenated nanotubes, nanotubes are separated by 10 Å. We use an integration scheme for the Brillouin zone with four k-points sampling along the tube axis. More k-point sampling did not change the total energy appreciably.

Results and Discussion

A. Hydrogen Adsorption at Coverage of 0.1. We first search for the relative stability of various adsorption patterns at $\theta = 0.1$. Hydrogen atoms are initially placed about 2 Å away from the top of the carbon atoms on the tube wall along the tube axis and relaxed fully with carbon atoms at the tube, using the conjugate gradient scheme implemented in the SCC-DFTB method. We define here various energies to characterize the adsorption nature and structural distortion. Adsorption energy per hydrogen atom is defined as the energy obtained during adsorption and can be calculated

$$E_{ad} = [E_{tot}(\text{H}-\text{CNT}) - E_{tot}(\text{pure CNT}) - n_H E_{self}(\text{H})]/n_H$$

where E_{tot} and E_{self} are the total energy of a given system and atomic self-energy, respectively, and n_H is the number of hydrogen atoms. The strain energy, which is the C−C bond distortion energy upon adsorption, is calculated

$$E_s = E_{tot}(\text{strained CNT without H}) - E_{tot}(\text{ideal CNT})$$

Figure 1 shows the cross sections of the fully relaxed geometry of the hydrogenated (5,5) armchair tube at various adsorption patterns at $\theta = 0.1$. As listed in Table 1, Figure 1d shows the lowest adsorption energy compared to those of the rest of the isomers. This agrees with the previous report that the pair formation is more favorable than the separated one.[26] Such an energy gain in Figure 1d could be attributed to the five strained C−C back-bonds compared to six C−C back-bonds of other types of isomers. However, the strain energies per carbon atom are very similar. We note that the bond angles around the hydrogen sites show values close to a tetrahedral bond angle of 109.5°, particularly in Figure 1d, as listed in Table 1. This indicates that the sp^3 hybridization is the main factor of the energy gain rather than the minimization of the strain energy. From this analysis, we consider only the pair adsorption for higher hydrogen coverage.

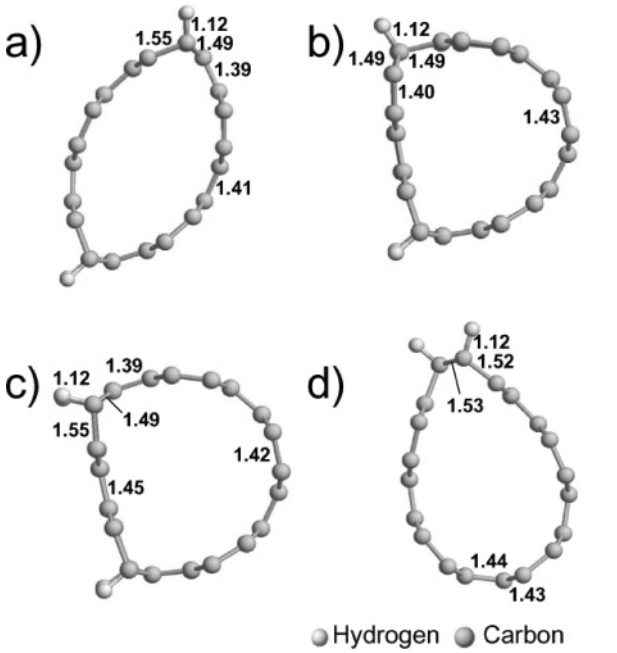

Figure 1. The cross-sectional views of the hydrogenated (5,5) nanotubes with various adsorption patterns at $\theta = 0.1$: (a−c) the second nearest neighbor configurations among hydrogen atoms and (d) the first nearest neighbor configuration. All bond lengths are given in units of Å.

TABLE 1: Various Parameters Determined from the SCC-DFTB Method for the Isomer Types, Indicated in Figure 1, and Bond Angles

isomer type	E_{ad} (eV/H)	E_S (eV/C)	∠HCC (deg)	∠CCC (deg)
a	−1.05	0.32	109.4, 111.4	105.8, 112.7
b	−0.78	0.32	109.1, 110.8	106.9, 111.6
c	−0.85	0.31	106.4, 110.3	108.1, 111.6
d	−1.77	0.31	108.8, 109.8	108.1, 110.7

B. Hydrogen Adsorption at Coverage $\theta \geq 0.2$. Figure 2 shows the cross sections of the fully relaxed geometry of the hydrogenated (5,5) armchair tube at various adsorption patterns at from $\theta = 0$ to 1. At all coverages, we searched for several adsorption patterns but only the most stable configurations are listed here. At $\theta = 0.2$, the circular cross section becomes elliptical due to the symmetry constraint, similar to that at $\theta = 0.1$. However, the adsorption energy was significantly lowered, as shown in Figure 3a, due to the doubling of sp^3 hybridization at two places. At coverage $\theta = 0.3$, the nanotube walls are rather graphitic by releasing the strain with a triangular polygonal shape. The adsorption energy should be lowered significantly for a similar reason as before but the energy gain is not as appreciable compared to the previous elliptical one at $\theta = 0.2$ due to the large local strain near the hydrogen sites, where all bond lengths are extended to near 1.53 Å, as shown in Figure 2d. The strain energy is plotted in Figure 3a.

The cross section looks more circular at $\theta = 0.5$. In this case, a heavy local strain is accumulated near the hydrogen sites and the bond angles (∠HCC = 106.5° and 105.6°) are also deviated from the tetrahedral bond angle, increasing the strain energy, as shown in Figure 3a. However, the C−C back-bonds prefer to have sp^3 hybridization evidenced by the bond angles (∠CCC = 108.8°) from the original sp^2 hybridization (∠CCC = 120°). This trend is similar for higher coverage, which is not shown here. At coverage $\theta = 1.0$, the circular cross section is still retained. The C−C back-bond lengths are extended to 1.52 Å (the bond direction deviated by 30° from the tube axis) and 1.58 Å (the bond direction perpendicular to the tube axis),

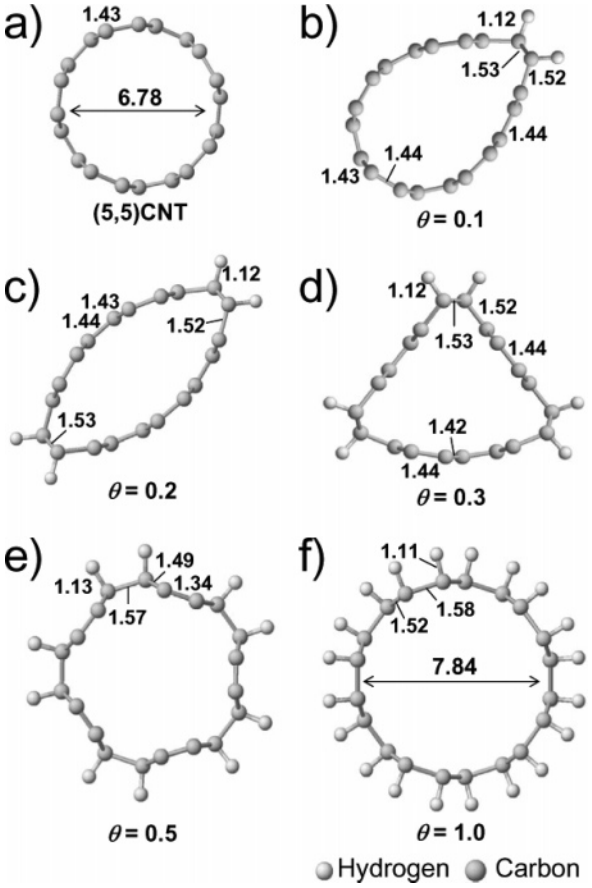

Figure 2. The cross-sectional views of the hydrogenated (5,5) nanotubes with various adsorption patterns at $\theta = 0$ to 1. All bond lengths are given in units of Å.

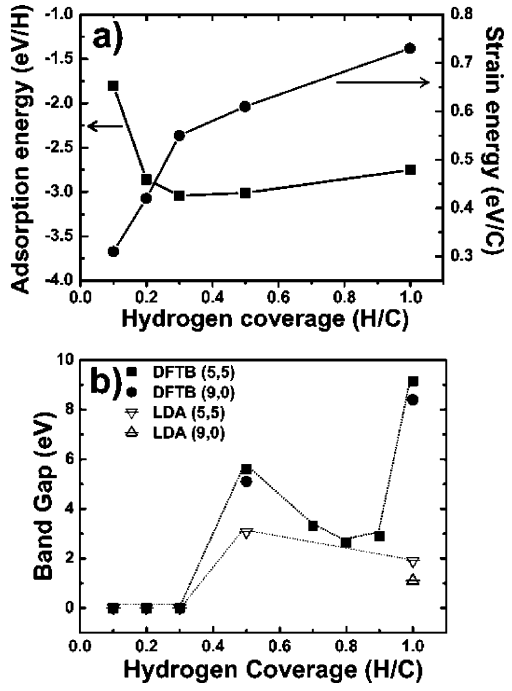

Figure 3. (a) Hydrogen adsorption energy and strain energy of carbon back-bonds and (b) band gap as a function of hydrogen coverage.

resulting in the maximum strain energy. The diameter is also expanded by 16% from that of the ideal SWCNT. We note that the energy loss compared to that of the half coverage is 0.26 eV/H, much smaller than 0.81 eV/H, calculated from the ONIOM method with clusters.[32] This is again attributed to the

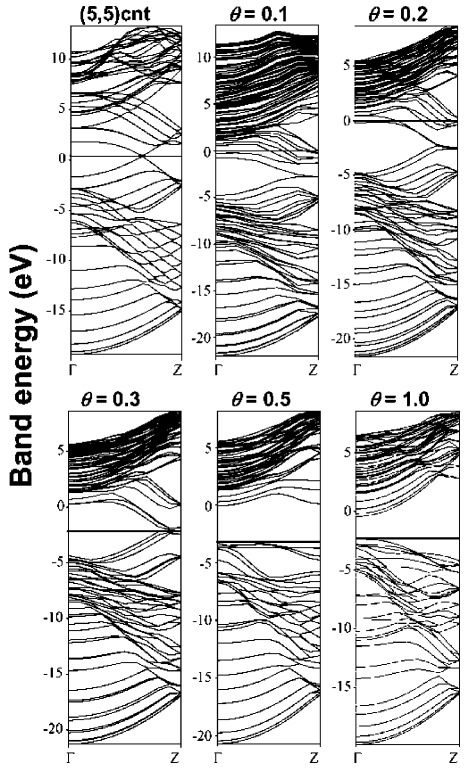

Figure 4. Band structures as a function of hydrogen coverage: Z (0, 0, π/2). The horizontal line indicates the Fermi level.

energy gain by the enhanced sp^3 hybridization particularly at carbon back-bonds ($\angle CCC = 108.9°$) at full coverage. Our calculations suggest that in addition to half coverage, the hydrogen adsorption model with higher coverage can also be suitable in experiment. One may also consider the buckled geometry for higher coverage that gives lower adsorption energy, similar to the previous work.[25] However, we limit our test to the hydrogen adsorption on the outer wall only in this paper, since this is more easily observable experimentally.

C. Electronic Structures. We next calculate electronic structures of previously optimized hydrogenated SWCNTs in Figure 2 as a function of coverage. Figure 4 shows the band structures at different coverage obtained by the LDA calculations. The (5,5) armchair SWCNT shows π and π^* band crossing at the Fermi level, revealing clearly metallic behavior. The stepwise van Hove singularities in the electronic density of states (EDOS) in the top panel of Figure 5 are characteristic of one-dimensional SWCNT. At lower hydrogen coverage $\theta < 0.5$, no forbidden band is allowed, indicating that the hydrogenated tubes are all metallic, as shown in Figure 5. The highly degenerate states in the conduction band are split into singlets due to the symmetry breaking, revealing a hydrogen-related prominent peak near 5 eV in the conduction band. This tendency becomes less severe with increasing coverage. Another hydrogen peak appears near −8 eV below the Fermi level in the valence band.

At hydrogen coverage $\theta = 0.5$, we see clearly a large band gap in the SCC-DFTB calculation opening of nearly 3.07 eV, which could be underestimated from the LDA. Such an underestimation is due to the incomplete basis sets in the SCC-DFTB method. This value is close to the experimentally observed value of 3.84 eV.[24] The π and π^* bands are removed by sp^3 hybridization, as explained in the previous section. The hydrogen-related peaks are split into two peaks near −1 and −5 eV below the Fermi level in the valence band and near 7 eV above the Fermi level in the conduction band, as shown in

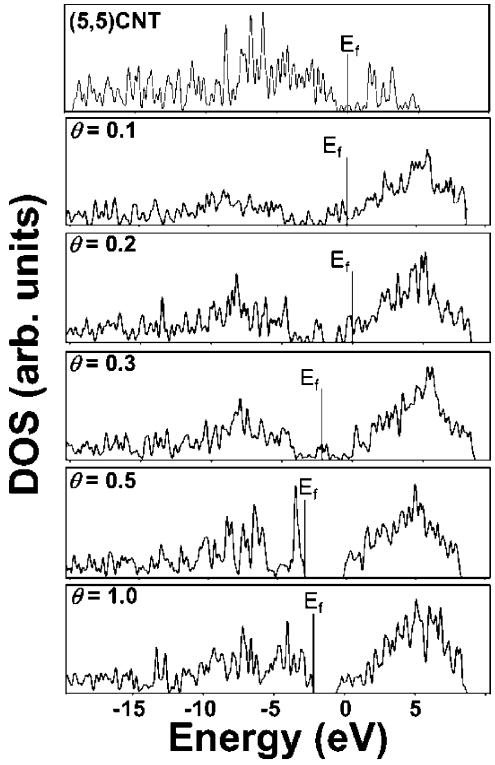

Figure 5. Electronic density of states as a function of hydrogen coverage. The vertical line indicates the Fermi level.

Figure 5. The peak positions at hydrogen coverage $\theta = 1.0$ are shifted to -2 eV and -6 eV below the Fermi level in the valence band. The band gap is reduced to 1.91 eV, as shown in Figure 3b. This is related to less symmetry breaking at full coverage, where the circular cross section is maintained, whereas the sp^3 hybridization is maximized at half coverage. Therefore, the band gap should be tailored by the degree of sp^3 hybridization, which is controlled by the hydrogen coverage. Figure 3b also shows the band gap changes calculated from the SCC-DFTB that were overestimated compared to the LDA results. Note that the symmetry of the hydrogenated nanotubes was changed from polygonal shapes to a perfect circular one by increasing coverage from 0.5 to 1.0. This abrupt change of the symmetry in the atomic structure may not be well-described by the SCC-DFTB due to the incomplete basis sets. The band gap opening of (9,0) zigzag nanotubes shows similar trends to those of the armchair tubes. The large band gap at $\theta = 1.0$ calculated from the SCC-DFTB does not follow the trend of the LDA calculations.

D. Junction Model. We next calculate a realistic junction model to explain the experimental observations of rectifying behavior in the hydrogenated nanotubes.[24] Half of the nanotube was covered by an SiO_2 layer and atomic hydrogen was exposed to the sample such that an abrupt junction was formed. Hydrogen atom hopping from top to sites requires an activation barrier of 1.65 eV.[26] Thus, the adsorption process at room temperature is rather determined by random-stochastic energetics. Figure 6a shows the junction model we adopted. Sixteen layers of (5,5) metallic tubes are used with periodic boundary conditions along the tube axis. Half of the SWCNT is covered by hydrogen atoms and becomes semiconducting with the band gap opening as described earlier. What we expect is the formation of a rectifier with a metal−semiconductor intramolecular junction, similar to the experimental situation with hydrogenation. One thing to note is that a sharp intramolecular junction is constructed with one strained monolayer at the interface. The C−C bond length

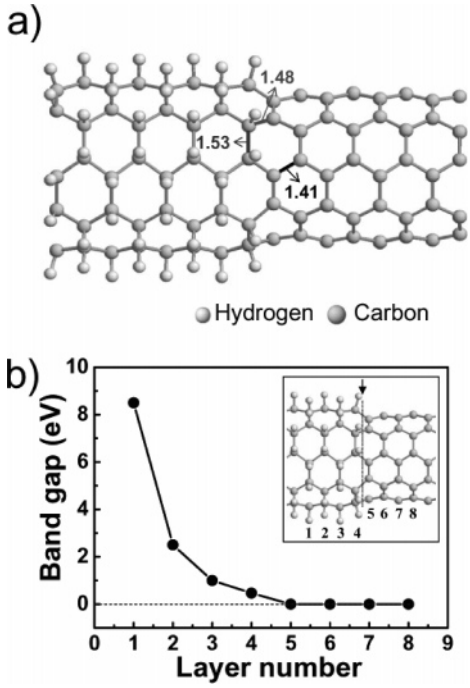

Figure 6. (a) The junction model with 16 layers, where half of the CNT is fully hydrogenated. (b) The local band gap calculated from the local EDOS as a function of layer numbers indicated in the inset. The arrow indicates the junction interface.

of the pure CNT is 1.42 Å and that of the hydrogenated CNT is 1.54 Å. The interface bond length is 1.48 Å, following the exact Vegard's rule. All other bond lengths from the first layer (layer numbers 4 and 5) with respect to the interface, indicated by an arrow, follow their own bond lengths. To our knowledge, this is the best intramolecular junction with a single strained layer at the interface. Figure 6b shows the local band gap calculated from the local electronic DOS near the interface. The layer number 5, the first layer at the pure metallic CNT side, shows zero band gap, inconsistent with the atomic configurations. On the other hand, the electronic structures of the hydrogenated CNT side are influenced by the metallic CNT side. The band gap is smeared up to three layers from the interface due to the charge transfer from the metallic CNT. The energy gap approaches 8.9 eV at the innermost layer. This suggests that we need to adopt a larger supercell than the current 16 layers to model the bulk transport phenomena as observed in experiments, since the band gap is close to 9 eV at infinite layers in our SCC-DFTB calculations, as shown in Figure 3b.

E. Instability of the CNT Walls with Hydrogen Adsorption at Low Coverage. So far we have discussed the stable adsorption geometries at low coverage up to $\theta = 0.5$. We can see from Figure 3 that the difference in the adsorption energy is not appreciable for coverages from $\theta = 0.2$ to 1.0. Although it has been reported that the coverage at $\theta = 0.5$ gives a more stable adsorption energy than at $\theta = 1.0$, the energy difference between them is within 0.3 eV/H in our calculations. Since the energy difference between structures is comparable to that of the LDA,[38] we believe that our approach is more reliable than the ONIOM method. Furthermore, the energy gain per hydrogen bond during adsorption is -3 eV/H, suggesting that the reaction is adsorption-dominant and the adsorption geometry with high hydrogen coverage of $\theta > 0.5$ can be realized in addition to that at low coverage.

What is more interesting is that all types of isomers at high coverage of $\theta > 0.5$ are stable, independent of the adsorption patterns, whereas the CNT walls can be disintegrated at low

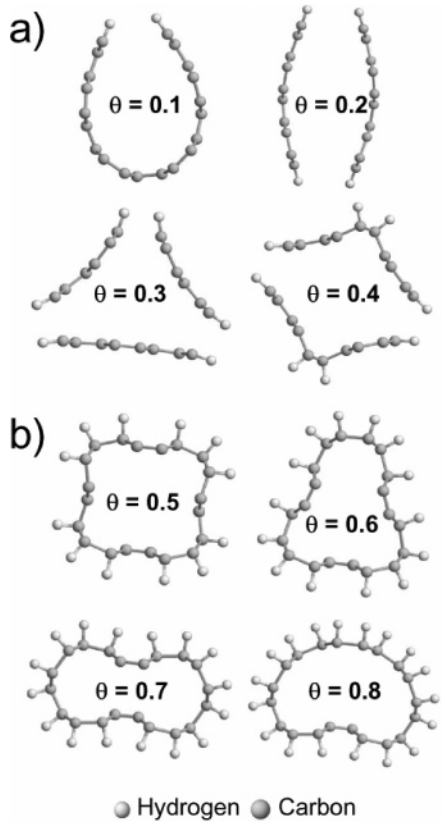

Figure 7. (a) Cross-sectional views of hydrogenated CNTs at low coverage up to $\theta = 0.4$. Typical examples of hydrogen adsorption that gives rise to disintegration of the nanotube wall. (b) Polygonal shapes of hydrogenated CNTs at high coverage from $\theta = 0.6$. Disintegration of the tube wall is not observed at high coverage, independent of the adsorption pattern.

coverage of $\theta < 0.5$, as shown in Figure 7. There are two carbon bond directions: One is perpendicular to the tube axis, which can be seen longer from the cross section in Figure 7, and another is oriented by 30 from the tube axis, which can be shorter. When two hydrogen atoms are attached on top carbon atoms with longer bonds at low coverage of $\theta < 0.5$, the C−C back-bonds can be exothermally broken. Instead the strains of the rest of the C−C back-bonds are released, making them nearly flat in most cases, as shown in Figure 7a. On the other hand, this type of disintegration is not observed in the hydrogen adsorption geometry at high a coverage of $\theta > 0.5$. At high hydrogen coverage, the local distortion induced by hydrogen adsorption is spread over all the carbon back-bonds. As a consequence, the circular cross sections become polygonal shapes with different symmetries but no disintegration is observed, as shown in Figure 7b. This implies that there is a chance that the CNTs can be destroyed probabilistically at an early stage of the hydrogenation adsorption process in experiments. Those which survived at an early stage with an appropriate adsorption pattern will be stable and can reach a high hydrogen coverage of up to $\theta = 1$, depending on the exposure time.

Conclusions

We have searched the stable adsorption geometries with different hydrogen coverage using SCC-DFTB and LDA methods: (i) We searched several stable adsorption geometries as a function of hydrogen coverage. The circular cross section becomes a polygonal shape with different symmetry at different coverage. (ii) We found that the hydrogen adsorption is stable in a wide range of coverage of $\theta \geq 0.2$ within the energy difference of 0.3 eV/H. (iii) We proposed that the band gap could be engineered with coverage changes, where the maximum band gap is obtained at half coverage. (iv) We constructed a rectifier by forming a metal−semiconductor intramolecular junction, where half of the nanotubes are covered by atomic hydrogen. A single strained monolayer at the interface is obtained, which is the most ideal junction model. (v) The CNT walls can be disintegrated particularly at an early stage of the hydrogenation process, depending on the adsorption patterns.

Acknowledgment. This work was supported by the MOST through the NRL program and in part by the KOSEF through CNNC at SKKU. We acknowledge the supercomputer center at Chonbuk National University for allowing us to use their computer.

References and Notes

(1) Dresselhaus, M. S.; Dresselhaus, G.; Saito, R. *Phys. Rev. B* **1992**, *45*, 6234.

(2) (a) Iijima, S. *Nature* (*London*) **1991**, *354*, 56. (b) Iijima, S.; Ichihashi, T.; Ando, Y. *Nature* (*London*) **1992**, *356*, 776.

(3) Hamada, N.; Sawada, S.; Oshiyama, A. *Phys. Rev. Lett.* **1992**, *68*, 1579.

(4) Mintmire, J. W.; Dunlap, B. I.; White, C. T. *Phys. Rev. Lett.* **1992**, *68*, 631.

(5) Collins, P. G.; Zettl, A.; Bando, H.; Thess, A.; Smalley, R. E. *Science* **1997**, *278*, 100.

(6) Fuher, M. S.; Nygård, J.; Shih, L.; Forero, M.; Yoon, Y.-G.; Mazzoni, M. S. C.; Choi, H. J.; Ihm, J.; Louie, S. G.; Zettl, A.; McEuen, P. L. *Science* **2000**, *288*, 494.

(7) Derycke, V.; Martel, R.; Appenzeller, J.; Avouris, Ph. *Appl. Phys. Lett.* **2002**, *80*, 2773.

(8) Javey, A.; Guo, J.; Paulsson, M.; Wang, Q.; Mann, D.; Lundstorm, M.; Dai, H. *Phys. Rev. Lett.* **2004**, *92*, 106804.

(9) Dillon, A. C.; Jones, K. M.; Bekkadahl, T. A.; Kiang, C. H.; Bethune, D. S.; Heben, M. J. *Nature* (*London*) **1997**, *386*, 377.

(10) Gordillo, M. C.; Boronat, J.; Casulleras, J. *Phys. Rev. Lett.* **2000**, *85*, 2348.

(11) Lee, J. Y.; An, K. H.; Heo, J. K.; Lee, Y. H. *J. Phys. Chem. B* **2003**, *107*, 8812.

(12) An, K. H.; Kim, W. S.; Jeon, K. K.; Park, Y. S.; Moon, J. M.; Lim, S. C.; Bae, D. J.; Lee, Y. H. *J. Electrochem. Soc.* **2002**, *149*, A1058.

(13) Jeong, S. Y.; Kim, J. Y.; Yang, H. D.; Yoon, B. N.; Choi, S. H.; Kang, H. K.; Yang, C. W.; Lee, Y. H. *Adv. Mater.* **2003**, *15* (14), 1172.

(14) Kong, J.; Franklin, N. R.; Zhou, C.; Chapline, M. G.; Peng, S.; Cho, K.; Dai, H. *Science* **2000**, *287*, 622.

(15) Yao, Z.; Postma, H. W. Ch.; Balents, L.; Dekker, C. *Nature* **1999**, *402*, 273.

(16) (a) Choi, W. B.; Lee, Y. H.; Lee, N. S.; Kang, J. H.; Park, S. H.; Kim, H. Y.; Chung, D. S.; Lee, S. M.; Chung, S. Y.; Kim, J. M. *Jpn. J. Appl. Phys.* **2000**, *39*, 2560. (b) Choi, W. B.; Chung, D. S.; Kang, J. H.; Kim, H. Y.; Jin, Y. W.; Han, I. T.; Lee, Y. H.; Jung, J. E.; Lee, N. S.; Park, G.-S.; Kim, J. M. *Appl. Phys. Lett.* **1999**, *75*, 3129.

(17) Mickelson, E. T.; Chiang, I. W.; Zimmerman, J. L.; Boul, P. J.; Lozano, J.; Liu, J.; Smalley, R. E.; Hauge, R. H.; Margrave, J. L. *J. Phys. Chem. B* **1999**, *103*, 4318.

(18) Kudin, K. N.; Bettinger, H. F.; Scuseria, G. E. *Phys. Rev. B* **2001**, *63*, 045413.

(19) An, K. H.; Heo, J. G.; Jeon, K. G.; Bae, D. J.; Jo, C.; Yang, C. W.; Park, C.-Y.; Lee, Y. H.; Lee, Y. S.; Chung, Y. S. *Appl. Phys. Lett.* **2002**, *80*, 4235.

(20) Park, K. A.; Choi, Y. S.; Kim, C. W.; Lee, Y. H. *Phys. Rev. B* **2003**, *68*, 045429.

(21) Wang, Q.; Johnson, J. K. *J. Phys. Chem. B* **1999**, *103*, 4809.

(22) Tada, K.; Furuya, S.; Watanabe, K. *Phys. Rev. B* **2001**, *63*, 155405.

(23) Chen, S.-P.; Chen, G.; Gong, X. G.; Liu, Z.-F. *Phys. Rev. Lett.* **2001**, *87*, 205502.

(24) Kim, K. S.; Bae, D. J.; Kim, J. R.; Park, K. A.; Lim, S. C.; Kim, J. J.; Choi, W. B.; Park, C. Y.; Lee, Y. H. *Adv. Mater.* **2002**, *14* (24), 1818.

(25) Lee, S. M.; An, K. H.; Lee, Y. H.; Seifert, G.; Frauenheim, Th. *J. Am. Chem. Soc.* **2001**, *123*, 5059.

(26) Bauschlicher, C. W., Jr. *Chem. Phys. Lett.* **2000**, *322*, 237.

(27) Gülseren, O.; Yildirim, T.; Ciraci, S. *Phys. Rev. Lett.* **2001**, *87*, 116802.

(28) Gülseren, O.; Yildirim, T.; Ciraci, S. *Phys. Rev. B* **2003**, *68*, 115419.
(29) Lee, E. C.; Kim, Y.-S.; Jin, Y.-G.; Chang, K. J. *Phys. Rev. B* **2002**, *66*, 073415.
(30) Andriotis, A. N.; Menon, M.; Srivastava, D.; Froudakis, G. *Phys. Rev. B* **2001**, *64*, 193401.
(31) Volpe, M.; Cleri, F. *Surf. Sci.* **2003**, *544*, 24.
(32) Bauschlicher, C. W., Jr. *Nano Lett.* **2001**, *1*, 223.
(33) Gülseren, O.; Yildirim, T.; Ciraci, S. *Phys. Rev. B* **2002**, *66*, 121401.
(34) Elstner, M.; Porezag, D.; Jungnickel, G.; Elsner, J.; Haugk, M.; Frauenheim, Th.; Suhai, S.; Seifert, G. *Phys. Rev. B* **1998**, *58*, 7260.
(35) Vanderbilt, D. *Phys. Rev. B* **1990**, *41*, 7892.
(36) Perdew, J. P.; Zunger, A. *Phys. Rev. B* **1981**, *23*, 5048.
(37) We tested the validity of the basis set. With a kinetic-energy cutoff of 20 Ry, the total energy difference in the model of $\theta = 0.5$ was 0.06 eV/atom, ensuring a safe use of a cutoff of 24 Ry.
(38) Lee, S. M.; Lee, Y. H. *Appl. Phys. Lett.* **2000**, *76*, 2877.